Effects on Spacecraft & Aircraft Electronics

Clive Dyer & David Rodgers,
Space Department, DERA Farnborough,
Hampshire GU14 0LX, UK

ABSTRACT

Spacecraft systems are vulnerable to Space Weather through its influence on energetic charged particle and plasma populations, while aircraft electronics and aircrew are vulnerable to cosmic rays and solar particle events. These particles produce a variety of effects including total dose, lattice displacement damage, single event effects (SEE), noise in sensors and spacecraft charging. Examples of all the above effects are given from observed spacecraft anomalies or on-board dosimetry and these demonstrate the need for increased understanding and prediction accuracy for Space Weather.

1. SPACE RADIATION ENVIRONMENT

1.1 Cosmic Rays

The earth's magnetosphere is bombarded by a nearly isotropic flux of energetic charged particles, primarily the nuclei of atoms stripped of all electrons. These comprise 85% protons (hydrogen nuclei), 14 % alpha particles or helium nuclei, and 1% heavier covering the full range of elements, some of the more abundant being, for example, carbon and iron nuclei. They travel at close to the speed of light, have huge energies (up to 10^{21} eV) and appear to have been travelling through the galaxy for some ten million years before intersecting the earth. They are partly kept out by the earth's magnetic field and have easier access at the poles compared with the equator. From the point of view of space systems it is particles in the energy range 1-20 GeV per nucleon which have most influence. An important quantity is the rigidity of a cosmic ray which measures its resistance to bending in a magnetic field and is defined as the momentum-to-charge ratio for which typical units are GV. The radius of curvature of the particle is then the ratio between its rigidity and the magnetic field. At each point on the earth it is possible to define a threshold rigidity or cut-off which a particle must exceed to be able to arrive there. Values vary from 0 at the poles to about 17 GV at the equator.

The influence of Space Weather is to provide a modulation in antiphase with the sunspot cycle and with a phase lag which is dependent on energy. The penetration of these galactic cosmic rays into the vicinity of the earth is influenced by conditions on the sun, which emits a continuous wind of ionised gas, or plasma, which forms a bubble of gas extending beyond the solar system. This carries out magnetic field lines from the sun and the strength of the wind and geometry of the magnetic field influence the levels of cosmic rays. At the present time (1998) we are just past the minimum in the eleven year solar cycle when the cosmic rays have easier access and are at their most intense.

1.2 Radiation Belts

The very first spaceflight of a radiation monitor in 1958 showed unusual regions of high counts and detector saturation which Van Allen identified as regions of radiation trapped in the earth's magnetic field. Subsequent research showed that these divide into two belts, an inner belt extending to 2.5 earth radii and comprising energetic protons up to 600 MeV together with electrons up to several MeV, and an outer belt comprising mainly electrons extending to 10 earth radii. The slot region between the belts has lower intensities but may be greatly enhanced for up to a year following one or two solar events in each solar cycle. The outer belt is naturally highly time variable and is driven by solar wind conditions. These variations are examples of Space Weather.

The earth's atmosphere removes particles from the radiation belts and low earth orbits can be largely free of trapped particles. However because of the displacement of the dipole term in the geomagnetic field away from the earth's centre, there is a region in the South Atlantic where the trapped radiation is found at lower altitudes. This is called the South Atlantic or Brazilian Anomaly (SAA) and dominates the radiation received by low earth orbits. In addition, highly inclined low earth orbits intersect the outer belt electrons at high latitudes in the so-called horn regions. An artist's impression of the radiation belts is given in figure 1, which shows how a high inclination orbit intersects the outer belt.
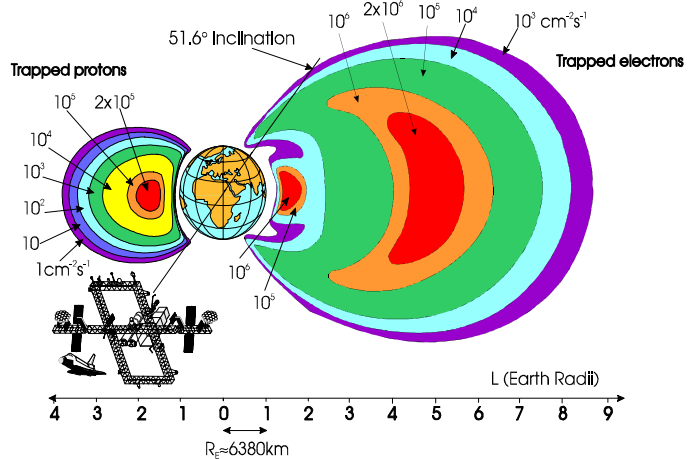

Figure 1. Artist's impression of the radiation belts.

As illustrated in section 3, Space Weather influences the upper atmosphere leading to variations in the particle population in the SAA.

1.3 Solar Particles

In the years around solar maximum the sun is an additional sporadic source of lower energy particles accelerated during certain solar flares and in the subsequent coronal mass ejections. These solar particle events last for several days at a time and comprise both protons and heavier ions with variable composition from event to event. Energies typically range up to several hundred MeV and have most influence on high inclination or high altitude systems. Occasional events produce particles of several GeV in energy and these can reach equatorial latitudes.

1.4 Atmospheric Secondaries

On the earth's surface we are shielded by the atmosphere. The primary cosmic rays interact with air nuclei to generate a cascade of secondary particles comprising protons, neutrons, mesons and nuclear fragments. The intensity of radiation builds up to a maximum at 60000 feet (this is known as the Pfotzer maximum after its discoverer who flew a detector on a very high altitude balloon in 1936) and then slowly drops off to sea level. At normal aircraft cruising altitudes the radiation is several hundred times the ground level intensity and at 60000 feet a factor three higher again. Solar particles are less penetrating and only a few events in each cycle can reach aircraft altitudes or ground level. Some of the neutrons are emitted by the atmosphere to give a significant albedo neutron flux at LEO spacecraft. The decay of these albedo neutrons into protons is believed to populate the inner radiation belt.

1.5 Spacecraft Secondaries

Spacecraft shielding is complicated by the production of secondary products. For example, electrons produce penetrating X-radiation, or bremsstrahlung, as they scatter and slow on atomic nuclei. Cascades of secondary particles, similar to those produced in the atmosphere, are also produced in spacecraft and can become very significant for heavy structures, such as Shuttle, Space Station and the large observatories, where path lengths can reach values equivalent to the atmospheric Pfotzer maximum (density x thickness values of around 100 g cm^{-2}).

2. RADIATION EFFECTS

2.1 Total Dose Effects

Dose is used to quantify the effects of charge liberation by ionisation and is defined as the energy deposited as ionisation and excitation per unit mass of material (note that the material should be specified). SI units are J/kg or grays (= 100 rads, where 1 rad is 100 ergs/g). The majority of effects depend on rate of delivery and so dose-rate information is required. Accumulated dose leads to threshold voltage shifts in CMOS due to trapped holes in the oxide and the formation of interface states. In addition increased leakage currents and gain degradation in bipolar devices can occur.

2.2 Displacement Damage

A proportion of the energy-loss of energetic radiation goes into lattice displacement damage and it is found that effects scale with NIEL, defined as the non-ionising energy loss per unit mass. The corresponding property of the radiation field is the non-ionising energy loss rate (i.e. per unit pathlength). For certain systems it is common to give the equivalent fluence of certain particles required to give the same level of damage (e.g. 1 MeV electrons or 10 MeV protons). Whereas dose is often measured directly, these quantities are usually calculated from measurements of the incident particle energy spectrum. Examples of damage effects are reduction in bipolar transistor gain, reduced efficiencies in solar cells, light emitting diodes and photodetectors, charge transfer inefficiency in charge coupled devices and resolution degradation in solid-state detectors.

2.3 Single Event Effects

The primary cosmic rays are very energetic and are highly ionising, which means that they strip electrons from atoms which lie in their path and hence generate charge. The density of charge deposition is proportional to the square of the atomic number of the cosmic ray so that the heavier species can deposit enough charge in a small volume of silicon to change the state of a memory cell, a one becoming a zero and vice versa. Thus memories can become corrupted and this could lead to erroneous commands. Such soft errors are referred to as single event upsets (SEU). Sometimes a single particle can upset more than one bit to give what are called multiple bit upsets (MBU). Certain devices could be triggered into a state of high current drain, leading to burn-out and hardware failure; such effects are termed single event latch-up or single event burn-out . In other devices localised dielectric breakdown and rupture can occur (single event gate rupture and single event dielectric failure). These deleterious interactions of individual particles are referred to as single event effects (SEE) to distinguish them from the cumulative effects of ionising radiation (total dose effects) or lattice displacements (damage effects). For space systems SEE have become increasingly important over the last fifteen years and are likely to become the major radiation effects problem of the future. For avionics SEE are the main radiation concern but total dose can be of significance for aircrew (although the latter is in fact an accumulation of SEE in tissue).

The severity of an environment is usually expressed as an integral linear energy transfer spectrum which gives the flux of particles depositing more than certain amount of energy (and hence charge) per unit pathlength of material. Energy deposited per unit pathlength is referred to as linear energy transfer (LET) and the common units are MeV per g cm^{-2} or per mg cm^{-2} (the product of density and pathlength). Devices are characterised in terms of a cross-section (effective area presented to the beam for a SEE to occur) which is a function of LET. For each device there is a threshold LET below which SEE does not occur. As device sizes shrink these thresholds are moving to lower LET and rates are increasing. In addition to directly ionising interactions with electrons, particles may interact with atomic nuclei thus imparting a certain recoil energy and generating secondary particles. Both the recoiling nucleus and secondary charged particles are highly ionising so that if such a reaction occurs in, or adjacent to, a device depletion region a SEE may result. Collisions with nuclei are less probable than collisions with orbital electrons but when certain particle fluxes are high this mechanism can dominate. This occurs in the earth's inner radiation belt where there are intense fluxes of energetic protons. It can also occur in the atmosphere where there is a build-up of significant fluxes of secondary neutrons. This mechanism is thought to be the dominant SEE hazard for current and near future avionics at most altitudes.

For radiation effects on biological systems it is found that there is a strong dependence on LET and so dose equivalents are used. Quality factors are defined to measure the enhancement in the effect compared with lightly ionising electrons or photons. These factors can be as large as 20 for heavy ions and fast neutrons. Thus for radiobiological dosimetry the charge deposition or LET spectrum must be measured, at least at coarse resolution, and summation of dose x quality factor made to give the dose equivalent, for which the SI units are sieverts (the dose equivalent of the rad is the rem, so that 1 sievert = 100 rem).

2.4 Background Noise in Sensors

Spurious counts are produced in many detector systems and these depend on the size distribution of individual depositions and can occur from both prompt ionisation and delayed depositions due to induced radioactivity

2.5 Electrostatic Charging

Surface charging can occur when spacecraft are bathed in energetic plasmas (several keV electron temperature) without the presence of neutralising cold plasma. This can occur in the geomagnetic tail region during geomagnetic storms and the subsequent discharges can couple into spacecraft systems. Internal charging, or deep dielectric charging as it is commonly called, can occur during energetic (several MeV) electron enhancements. Electrons penetrating the thin skin can be trapped in dielectric materials near the surface and sufficient build-up can occur over a few days to result in a damaging electron caused electromagnetic pulse (ECEMP).

3. EXAMPLES OF EFFECTS AND SPACE WEATHER

3.1 Total Dose

It is difficult to obtain hard evidence of failures as there are usually insufficient diagnostics and effects are readily confused with ageing. Exceptions are when deliberate experiments are performed, such as on the Combined Release and Radiation Effects Spacecraft (CRRES) or the current Microelectronics and Photonics Test Bed. Sensitive pMOS transistors are frequently used as RADFETs to deliberately monitor the accumulated dose via the measured threshold voltage shift.

Example measurements from the CREDO monitor flown on APEX (352x2486 km, 70° inclination) and STRV (GTO, 7° inclination) are given in figure 2. Dose-rate variations for the most exposed dosimeters on APEX and STRV are compared for the first 90 days of APEX operation commencing in August 1994, after which extensive interruptions to the power supply rendered the data difficult to interpret. The underlying downward trend seen on APEX during the first 60 days is due to the precession of apogee away from the equator, where maximum penetration of the inner belt occurs. This trend is well predicted by the standard AE-8/AP-8 models of trapped electrons and protons (Refs. 1 & 2). However the least shielded dosimeter also shows periodic large increases in dose-rate coincident with increases seen by STRV as well as electron fluxes seen at geostationary orbit by GOES-7, showing that enhancements in the outer radiation belt are observable at low altitude in the high latitude "horn regions". This is a clear

example of Space Weather simultaneously affecting dose rates in GEO,GTO and MEO orbits.
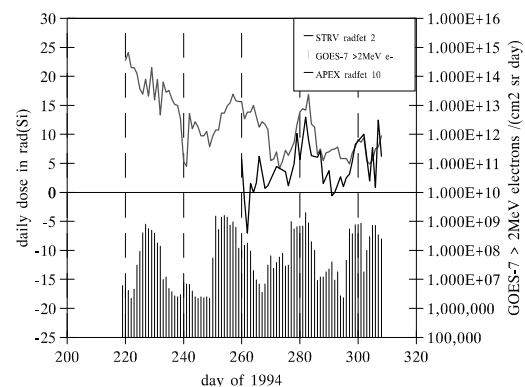

Figure 2. Dose-rates (upper plot) on APEX (eccentric LEO to 2400 km) and STRV (GTO) are compared with electron fluxes measured on GOES in GEO (lower histogram).

3.2 Displacement Damage

The clearest examples arise from observations of degradations in solar array efficiency where sharp drops can occur during solar particle events. For example, drops in efficiency of 4% in GEO (Ref. 3) and 2% in LEO (Ref. 4) were observed during the large solar particle events of September and October 1989. The March 1991 event was responsible for removing the equivalent of 3 years lifetime from the GOES spacecraft (Ref. 5)

Recently optocoupler failures have been observed on the TOPEX spacecraft due to reduced current transfer efficiency resulting from proton damage of the photodetector element (Ref. 6). Such failures will be susceptible to Space Weather through variations in the inner belt protons and solar protons.

3.3 Single Event Effects

A classic example of cosmic-ray induced upsets was experienced by the NASA/DoD Tracking and Data Relay Satellite (TDRS-1) which incorporated sensitive RAM chips in the Attitude Control System. Rates of 1 to 2 per day clearly showed modulation with cosmic rays, while during the solar particle events of September to October 1989 rates reached 20 per day (Ref. 7). As a result expensive ground control procedures had to be employed on what was intended to be an autonomous spacecraft.

A classic example of hardware failure occurred in the PRARE (Precision Ranging Experiment) instrument carried on the ERS-1 (European Remote Sensing Spacecraft). A latch-up failure occurred in the heart of the SAA after 5 days and led to loss of the instrument. Subsequent analysis and ground testing proved this diagnosis (Ref.8).

Commercial, unhardened systems are particularly vulnerable. For example IBM ThinkPad computers on the MIR Space station have shown upsets every nine hours (Ref. 9), while other laptop computers on Space Shuttle have shown upset rates of one per hour (Ref. 10)

Examples will be given to show how Space Weather influences the SEE environment from sea level to interplanetary space.

3.3.1 Avionics

In the last ten years it has been realised that single event effects will also be experienced by sensitive electronics in aircraft systems, which are subjected to increasing levels of cosmic radiation and their secondaries as altitude increases. Significant effort has gone into monitoring the environment and analysing operational systems for SEUs.

The CREAM (Cosmic Radiation Effects and Activation Monitor) and CREDO (Cosmic Radiation Effects and Dosimetry) detectors are designed to monitor those aspects of the space radiation environment of concern for electronics; i.e. charge-deposition spectra, linear energy transfer spectra and total dose. In the CREAM and CREDO-I instruments the SEU environment is monitored by means of pulse-height analysis of the charge-deposition spectra in ten pin diodes, each 1 cm^2 in area and 300 µm in depth.
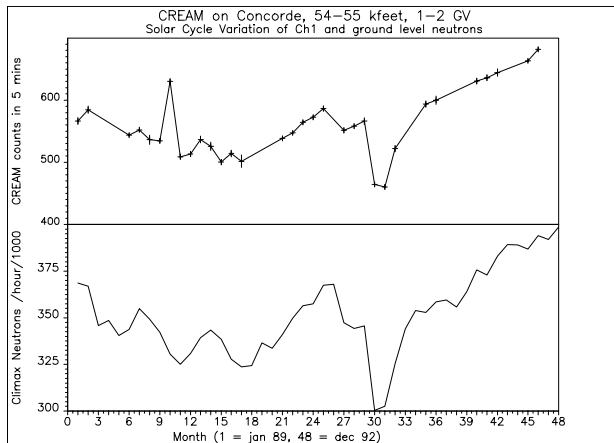
Figure 3. Monthly mean count rates from CREAM on Concorde from Jan 89 to Dec 92 compared with ground level neutron monitor at Climax.

A version of the CREAM detector made regular flights on-board Concorde G-BOAB between November 1988 and December 1992. Results from 512 flights have been analysed of which 412 followed high latitude transatlantic routes between London and either New York or Washington DC (Ref. 11). Thus some 1000 hours of observations have been made at altitudes in excess of 50000 feet and at low cut-off rigidity (< 2 GV) and these span a significant portion of solar cycle 22. Figure 3 shows the count rate in CREAM channel 1 (19fC to 46fC, LET 6.1 MeV cm^2 g^{-1}) plotted as monthly averages for the ranges 54-55 kfeet and 1-2 GV. The rates show a clear anticorrelation with the solar cycle and track well with the neutron monitor at Climax Colorado (altitude 3.4 km, cut-off rigidity 2.96 GV). The enhanced period during September and October 1989 comprised a number of energetic solar particle events observed by ground level, high latitude neutron monitors and the Concorde observations are summarised in Table 1 (Refs. 12 & 13), which gives the enhancement factors compared with adjacent flights when only quiet-time cosmic rays were present.

Table 1
Enhancement factors for CREAM on Concorde
during solar particle events

Channel Number	29-Sep 1406 - 1726	19-Oct 1420 - 1735	20-Oct 0859 - 1204	22-Oct 1814 - 2149	24-Oct 1805 - 2135
1	3.7 ± 0.02	1.6 ± 0.01	1.4 ± 0.01	1.5 ± 0.01	3.4 ± 0.01
2	4.9 ± 0.1	1.9 ± 0.04	1.6 ± 0.04	1.8 ± 0.04	4.5 ± 0.06
3	5.7 ± 0.1	2.1 ± 0.07	1.8 ± 0.07	1.9 ± 0.07	5.2 ± 0.1
4	5.9 ± 0.2	2.0 ± 0.1	1.8 ± 0.1	2.0 ± 0.1	5.7 ± 0.2
5	5.6 ± 0.6	2.0 ± 0.3	2.0 ± 0.4	2.1 ± 0.3	4.9 ± 0.4
6	6.1 ± 1.5	3.0 ± 0.7	1.1 ± 0.8	1.0 ± 0.6	4.3 ± 1.1
7	(17.4 ± 17.4)	-	(30.4 ± 30.4)	-	-
8	-	-	-	-	-
9		-	-	-	-

More recently the CREAM detector has been operated on a Scandinavian Airlines Boeing 767 operating between Copenhagen and Seattle via Greenland, a route for which the cut-off rigidity is predominantly less than 2 GV. Approximately 540 hours of data accumulated between May and August 1993 have been analysed and these are combined with Concorde data from late 1992 to give the altitude profiles of counts for channel 5 shown in figure 4. Also plotted are predicted rates from cosmic rays and their secondary fragments using the AIRPROP code (Ref. 14) showing that these are not the major contribution. Recent work (Ref. 15) has concentrated on explaining both the altitude dependence and the energy deposition spectra using radiation transport codes. The results of a microdosimetry code extension to the Integrated Radiation Transport Suite are shown in figure 4. This microdosimetry code tracks the products of nuclear reactions occurring in the sensitive volume of silicon and its surrounds. Figure 4 shows that atmospheric secondary neutrons are the major contribution but that ions start to become important at the highest altitudes.
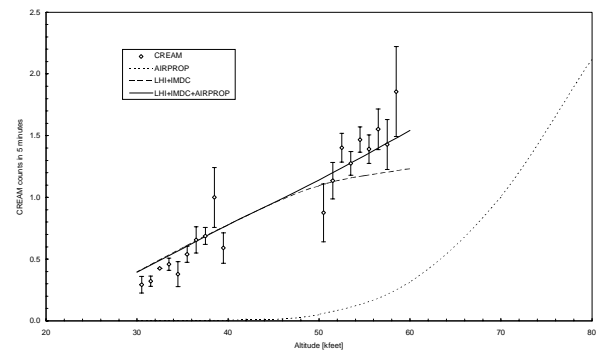

Figure 4. Average CREAM channel 5 count rates as a function of altitude at 1-2GV from SAS & Concorde flights. Also shown are the predictions from AIRPROP and from neutron interactions as calculated using radiation transport and microdosimetry codes (LHI+IMDC). Neutrons dominate at 30 to 40 kfeet but cosmic ray ions start to contribute at supersonic altitudes.

An increasing body of data on upsets in avionics systems is being accumulated. In an unintentional experiment, reported by Olsen et al. (Ref. 16), a commercial computer was temporarily withdrawn from service when bit-errors were found to accumulate in 256 Kbit CMOS SRAMs (D43256 A6U-15LL). Following ground irradiations by neutrons, the observed upset rate of 4.8x10^{-8} upsets per bit-day at conventional altitudes

(35000 feet) was found to be explicable in terms of SEUs induced by atmospheric neutrons. In an intentional investigation of single event upsets in avionics, Taber and Normand (Ref.17) have flown a large quantity of CMOS SRAM devices at conventional altitudes on a Boeing E-3/AWACS aircraft and at high altitudes (65000 feet) on a NASA ER-2 aircraft. Upset rates in the IMS1601 64Kx1 SRAM varied between 1.2×10^{-7} per bit-day at 30000 feet and 40° latitude to 5.4×10^{-7} at high altitudes and latitudes. Reasonable agreement was obtained with predictions based on neutron fluxes.

3.3.2 Shuttle

The CREAM detector has flown on a number of Shuttle missions between 1991 and 1998.
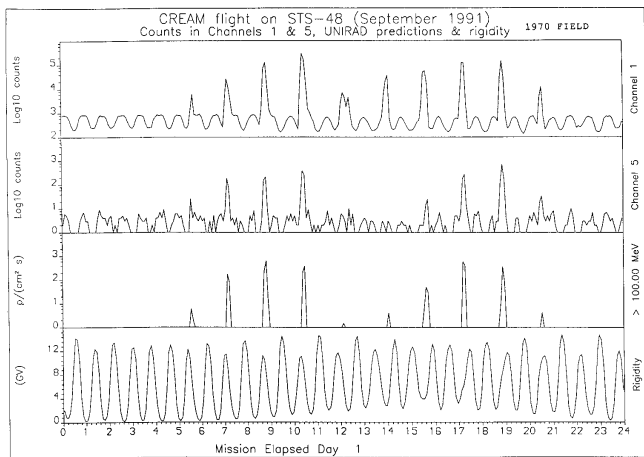
Figure 5. Count-rate profile for CREAM on STS-48 compared with prediction based on AP-8 & 1970 magnetic field model. Double-peak pass at orbit 23 is not predicted.

Figure 5 show count-rate profiles for a typical day in the mission STS-48 which was launched on 12 September 1991 into a 57°, 570 km orbit. The cosmic-ray modulation around the orbit due to the geomagnetic cut-off rigidity is seen while the peaks are due to passages through the SAA regime of trapped protons. Rates are compared with predicted proton fluxes based on the AP-8 model in conjunction with the 1970 geomagnetic field model and with cut-off rigidities obtained using the CREME code (Ref. 18). It can be noted that peak observed at orbit 23 is not predicted However use of the 1991 geomagnetic field does predict a peak for this orbit. While use of the field pertaining to the data from which the models were created is the recommended procedure it does not account for the steady drift of the SAA contours to the West due to evolution of the geomagnetic field. This is illustrated in figure 6 where the ground track of orbit 23 for STS-48 is shown with respect to the SAA contours obtained using the 1991 field. it can be seen that the orbit just clips the contours to the Southwest and would miss for 1970 field contours. For this orbit there is a second peak observed off of South Africa which is not predicted by either field model. This region is where the L=2.5 shell intersects this altitude orbit and the high fluxes are due to the second proton belt observed by CRRES to be created by the solar flare event of 23 March 1991. Careful analysis of STS-53 data obtained in December 1992 again shows a small enhancement in this region when cosmic-ray contributions are carefully subtracted. This was originally believed to be the remnants of the March 1991

event but evidence from UoSAT-3 (see below) now points towards a second enhancement, possibly associated with a flare in October 1992. A recent review of Shuttle results is given in Ref. 19 and shows further SAA movement which cannot be predicted by simply updating the field model used with AP8.
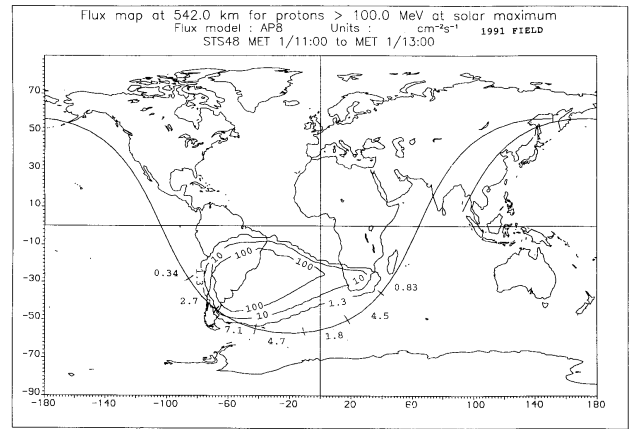

Figure 6. Ground track of orbit 23 for STS-48 is shown with respect to proton flux contours (E > 100 MeV) from AP-8 & 1991 field. With the updated field the orbit intersects the SAA. An additional peak is seen off of South Africa due to the new radiation belt created in March 1991.

In figure 7 cosmic-ray counts in channel 1 are plotted against rigidity for six missions spanning September 1991 (STS-48) to May 1997 (STS-84). The increase in the low latitude counts by more than a factor of two clearly shows the declining phase of the solar cycle leading to more cosmic rays at the low rigidity end of the spectrum while the high rigidity end remains unaltered.
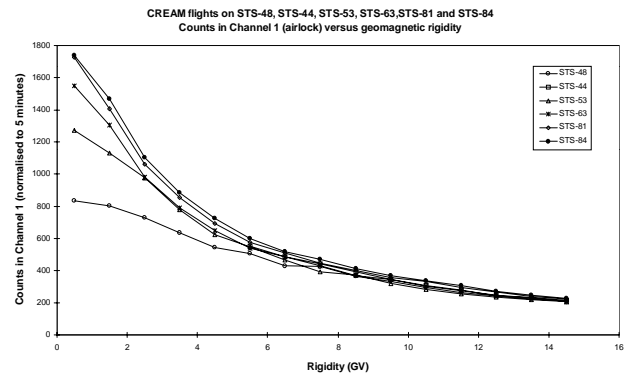

Figure 7. Channel 1 count rates from CREAM as a function of rigidity for Shuttle missions spanning Sept 1991 to May 1997 showing the increase at high latitudes but little variation at low latitudes.

3.3.3 UoSAT Series

This series of microsatellites (50-60 kg) has been developed by the University of Surrey to provide low cost access to space for a variety of applications such as store-and-forward communications. All are in low earth orbit with altitudes between 700 and 1300 km and have included an evolving range of large solid-state memories comprising commercial

components. These have yielded a wealth of data on single event upsets and multiple-bit upsets, while use of Error Detection and Correction (EDAC) procedures has allowed the continued successful operation of the spacecraft. Following the realisation of the significance of the SEU data from UoSAT-2 the later spacecraft in the series have included the radiation monitors CREDO provided by DERA and the similar Cosmic Ray Experiment (CRE) produced at Surrey.

UOSAT-2 was launched in 1984 into a 700 km, near polar, sun-synchronous orbit. Following the realisation of the significance of the data the SEUs have been logged to within 8.25 minutes accuracy since 1988. Data have been presented in (Ref. 20) from which figure 8 shows that the majority of events occur in the SAA region, while a further contribution from cosmic rays is seen to cluster at high latitudes. In addition the flare event of October 1989 gave a large increase in upsets.
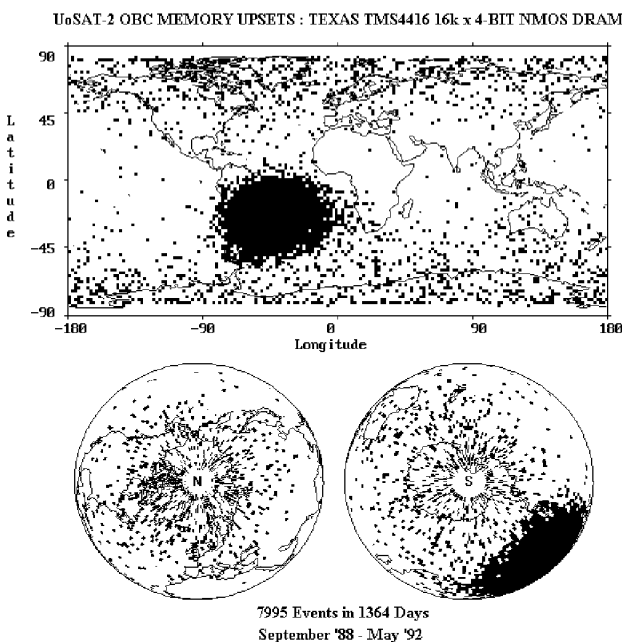

Figure 8. Geographical distribution of SEUs in nMOS DRAMs on UoSAT-2 showing clustering of proton events in the SAA and cosmic-ray events at high latitude.

The interest in such SEU data led us to develop the CREAM instrument developed for Concorde and Shuttle into the CREDO instrument for free-flyers and this was first launched on UoSAT-3 into 800km, 98.7° orbit in January 1990. Continuous data on both environment and upsets have been obtained since April 1990 until October 1996, covering conditions ranging from solar maximum to minimum and including a large number of solar flare events, the most notable of which was the March 1991 event responsible for creating the new proton belt as observed by CRRES.
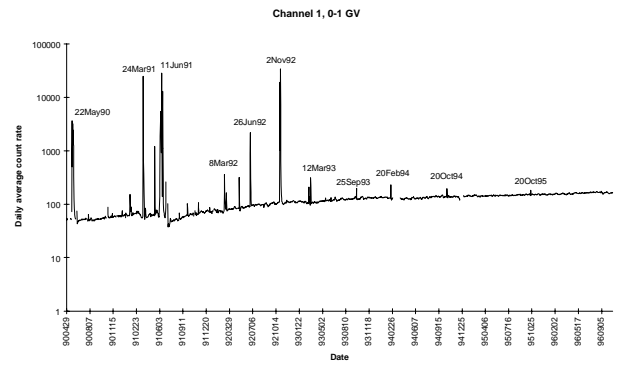

Figure 9. High latitude counts from CREDO on UoSAT-3 showing cosmic ray modulation and solar particle events.

Figure 9 shows the time variation in the high latitude channel-1 count rate of the CREDO instrument up until October 1996. South Atlantic Anomaly passes are removed from these data. The underlying increase with decreasing solar activity can be clearly seen as can the solar particle events which steadily diminished in number and intensity as solar minimum was approached. The SAA proton fluxes have also evolved over this time and the daily accumulated counts in the SAA region are shown as a function of time in figure 10 taken from Ref. 21. The flux actually fell during the first 2 years reaching a broad minimum in 1992 before steadily increasing by 34%. This is due to decreased atmospheric losses as the upper atmosphere contracts towards solar minimum but there is an obvious phase lag due to the removal time. The increase of 34% may be compared with the predicted increase between AP-8MAX and AP-8MIN which is 24% for this altitude. Given that the maximum fluxes were still not attained in late 1996, it is evident that atmospheric modulation effects are greater than predicted by AP-8. Contour plots obtained in 1992 and 1995 are compared in figure 11 and show both a general increase in intensity, as discussed above, and a north-westward drift due to the evolution of the geomagnetic field.
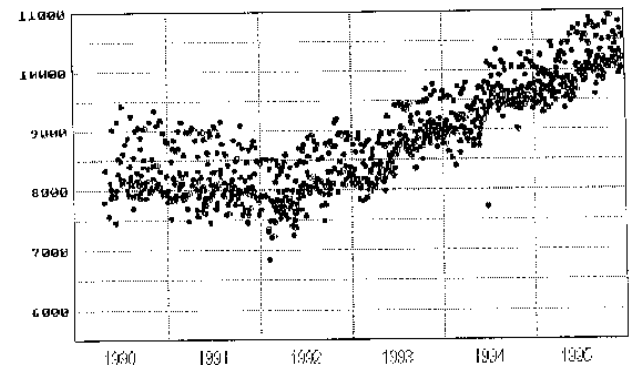

Figure 10. UoSAT-3 daily accumulated CREDO channel 1 counts in the SAA region.

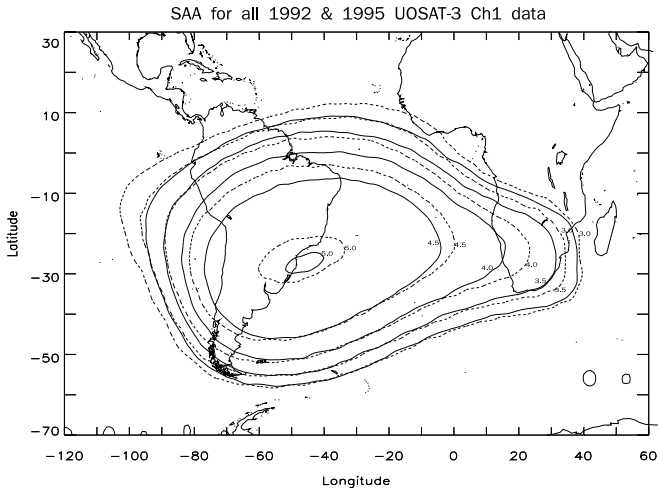SAA for all 1992 & 1995 UOSAT-3 Ch1 data

Figure 11. Contour plots from channel 1 of CREDO on UoSAT-3 show both an increase and a north-westward drift in the SAA between 1992 (solid lines) and 1995 (dotted lines).
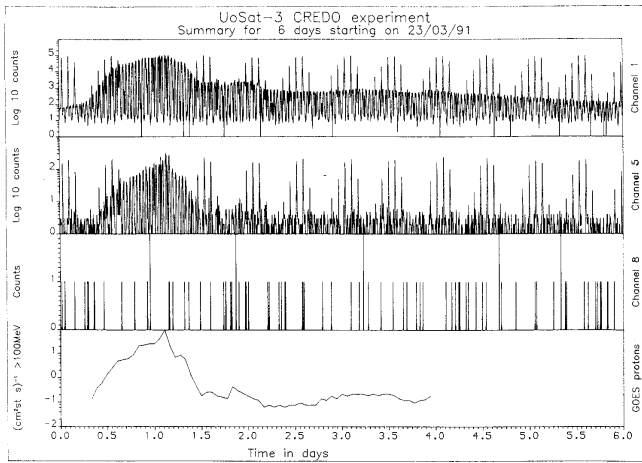

Figure 12. Count-rate profiles from CREDO on UoSAT-3 in March 91 show the flare particles at high latitude while GOES in GEO is continuously exposed.

The count-rate profiles are shown for the six-day period commencing on 23 March 1991 in figure 12 and comparison is made with the proton channel for energies greater than 100 MeV from the GOES instrument in geostationary orbit. The counts are modulated around the orbit and the contribution of the solar flare is seen as the high latitude envelope of the count rate which reaches levels comparable to those from the SAA (seen as groups of spikes before and after the flare peak). The energy-deposition spectra during the event are compared with quiet-time for the same rigidities as above in figure 13. A significant enhancement is seen at 2-3 GV, whereas the standard CREME predictions show no penetration to these rigidities. This is probably an example of cut-off suppression by the geomagnetic storm. Comparison has now been made with the CREME96 model, based on the October 1989 event, and this is presented in figure 14. Orbit-averaged data and predictions are compared and the two CREME96 predictions are with (S) and without (NS) storm suppression of the geomagnetic cut-offs. Similar comparisons are made for the events of 31 October to 2 November 1992 in figure 15. It can be seen that the October 89 event provides a suitably conservative overestimate for all events seen by UoSAT-3. The overestimate is particularly marked at high LET, showing this event to be particularly rich in heavy

ions. Only the November 92 event shows a significant enhancement at high LET. In general proton-induced upsets will more significant than flare heavy ions, although the occasional event, such as October 1989, means that they must be taken into account (Ref. 22).
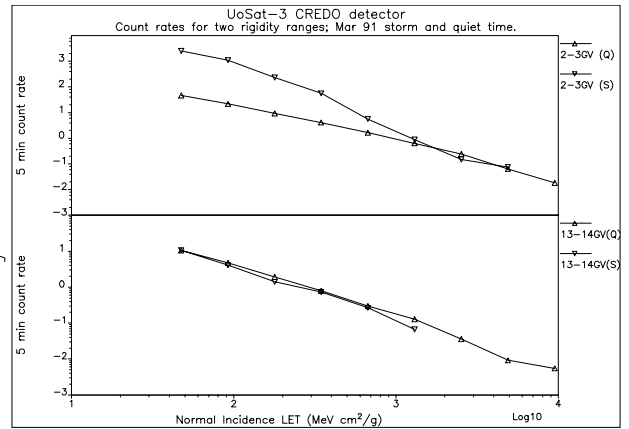

Figure 13. Energy-deposition spectra during the March 91 event (S) compared with quiet-time (Q) at low and high rigidities. The penetration to 2-3 GV is unexpected.
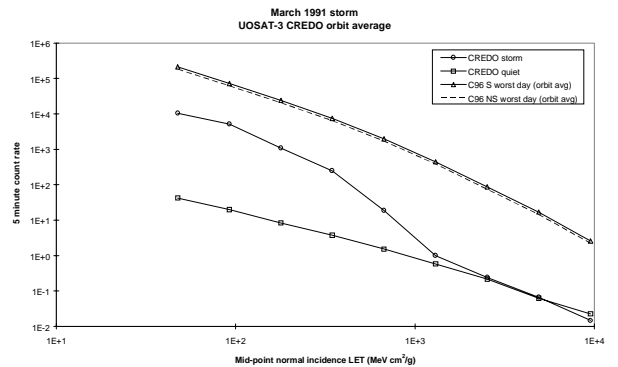

Figure 14. Orbit-averaged CREDO energy-deposition spectrum on worst day of March 1991 event is compared with preceding quiet time data and CREME96 prediction for a solar particle event worst day. The latter is given for storm suppression of geomagnetic cut-off (S) and for normal cut-offs (NS). This has little difference for orbit averages at this inclination.
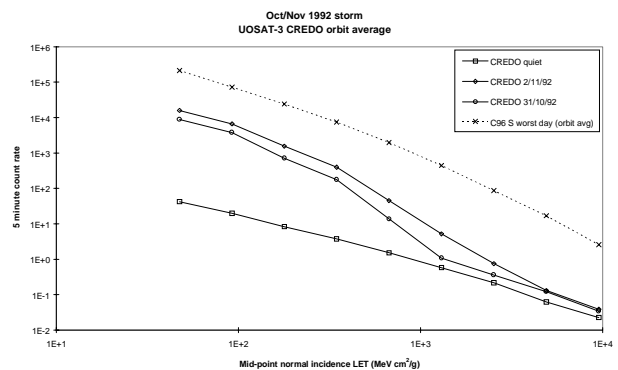

Figure 15. As figure 14 but for worst days of October and November 1992 events. The November event has a higher LET component from heavy ions.

The March 1991 event was responsible for a long-lived enhancement in trapped protons at around L=2.6 as observed by

CRRES until its demise in October 1991. As discussed above, increases in this region were seen from the high inclination Shuttle missions STS-48 and STS-53 in September 1991 and December 1992 respectively. The CREDO detector on UoSAT-3 has the advantage of continuous coverage during this time period, although the orbit gives only short duration passages through the regime of interest. The UoSAT data have been carefully examined by mapping the count-rates into B-L space following subtraction of cosmic-ray contributions by means of fits to cosmic-ray counts obtained at identical geomagnetic latitudes outside of the belts. In addition days containing direct solar-flare particles have been excluded based on data from the GOES spacecraft. The remaining counts taken over the B-L region of the new belt accessible to UoSAT have been averaged on a monthly basis and the resulting time variations for L values greater than 2.2 and 2.4 are plotted in figure 16 to show the time history of this region of the radiation belts. The marked increase at March 1991 and the decay through to October 1991 are clearly seen. There appears to have been a second increase in November 1992, possibly arising from the proton flare of 31 October 1992, and this was probably responsible for the enhancement seen by STS-53. There is also a hint of an enhancement early on following the May 1990 solar flare. Clearly the slot region is highly dynamic.
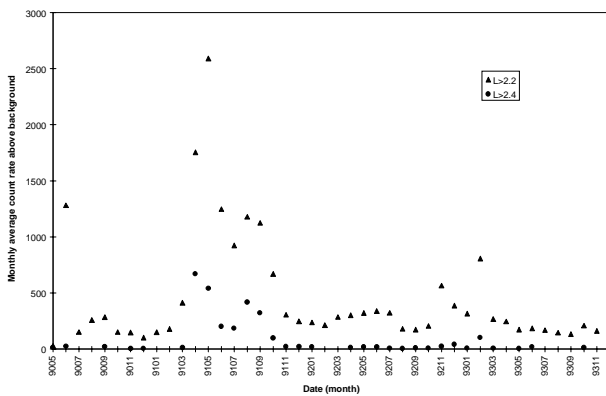

Figure 16. Monthly-averaged count rates at L>2.2 & 2.4 from UoSAT-3 with cosmic-ray background subtracted show new regimes of trapped radiation following flare events in March 91 and October 92.

3.3.4 CRRES

The Combined Release and Radiation Effects Spacecraft (CRRES) was the most comprehensively instrumented spacecraft ever launched with the purpose of performing collateral measurements of the radiation environment and its effects on a wide range of state-of-the art and future electronics technologies. Nineteen radiation experiments on-board included the microelectronics effects package, the internal discharge monitor, the gallium arsenide solar panel experiment and a wide range of particle detectors. This effort has been accompanied by extensive supporting ground tests and radiation environment modelling activities. The two-ton spacecraft was launched into a geostationary transfer orbit (350 x 33500 km, 18.1° inclination) on 25 July 1990 and operated until October 1991.

It was fortunate that the spacecraft was operational at the time of the March 1991 solar-particle event and geomagnetic storm and was able to observe the creation of a new radiation belt of both energetic protons (Ref. 23) and very energetic electrons (Ref. 24) at around L=2.5 and to monitor the subsequent fluxes and their influence on dose-rates (Ref. 25) and upsets. Large increases in both dose-rates and SEU rates were observed following the March event. Figures 17a and 17b, taken from Ref, 23 show the changed profile in upsets around the orbit following this event, while figure 18, taken from Ref. 24, shows the radical changes in proton and electron profiles before and after the event.
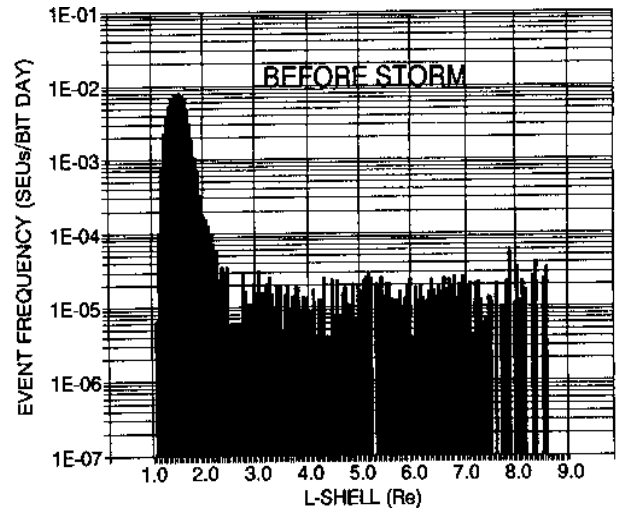

Figure 17a. SEU frequency for 35 proton-sensitive devices for the first 585 orbits (25 July 1990 to 22 March 1991) of CRRES are shown as a function of L-shell. The peak at L=1.5 coincides with the heart of the inner radiation belt (Ref. 23).
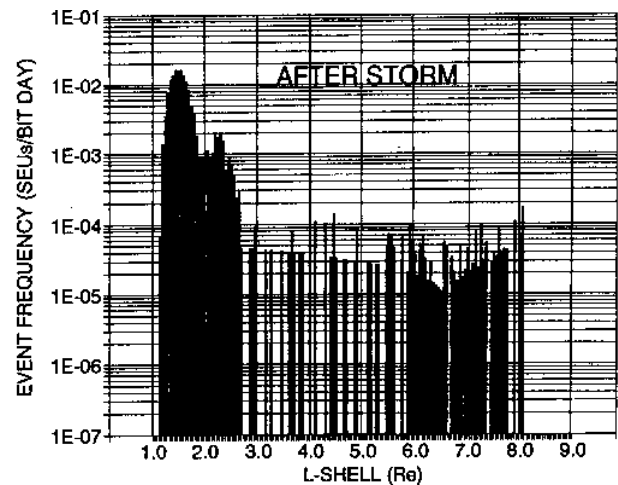

Figure 17b. As above but for the 141 orbits following the solar-proton event of 23-29 March 1991. The creation of a second proton belt leads to a peak at L=2.3 to 2.5

CRRES ORBIT 581   DAY 80 1991

p 20-80 Mev

e > 13 Mev

CRRES ORBIT 596   DAY 86 1991

p 20-80 Mev

e > 13 Mev

CRRES ORBIT 1001   DAY 257 1991
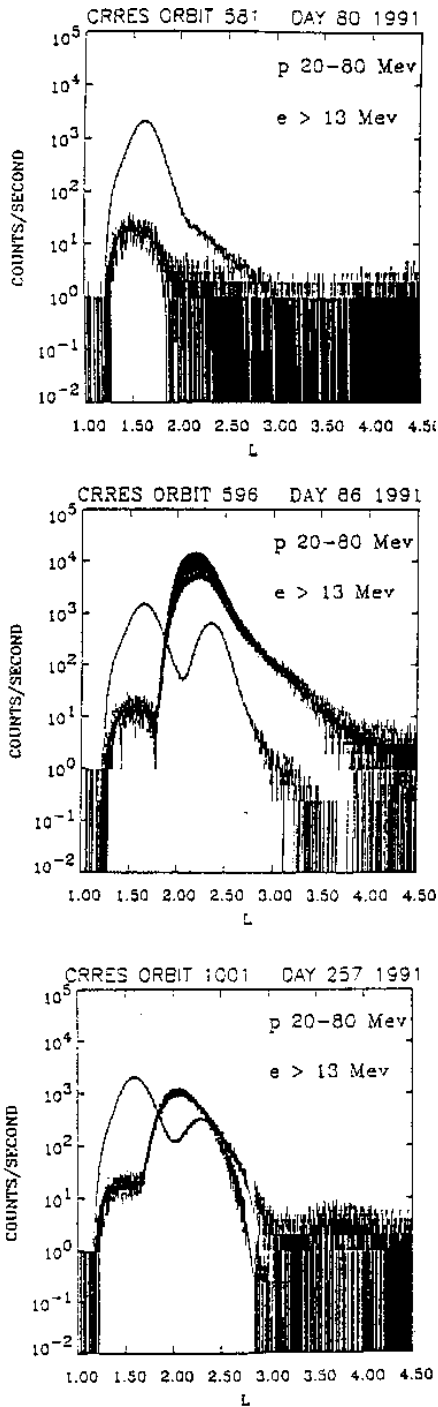
p 20-80 Mev

e > 13 Mev

Figure 18. The three panels show the radial profiles for the 20 to 80 MeV proton channel and the >13 MeV electron channel for an orbit just before the injection event, just afterwards, and six months afterwards. The major change in the energetic particle population caused by the electron event and the evolution of the particle population with time can be seen (Ref.24).

3.4 Background Noise in Sensors

Enhanced background rates in SOHO and IRAS detectors due to cosmic rays, spacecraft secondaries and solar particle events are discussed elsewhere in these proceedings. Gamma-ray and X-ray detectors are particularly sensitive to background including delayed events from induced radioactivity (Refs.26&27). Figure 19 shows the predicted enhanced emission of gamma rays from the XMM spacecraft during a solar particle event. These interact with the CCD detectors to give increased background counts in the instrument bandwidth (Ref. 27).
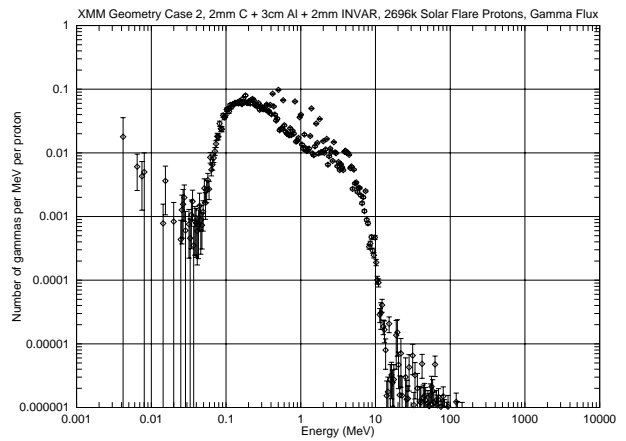

Figure 19. Solar-proton induced gamma-ray emissions in XMM

3.5 Spacecraft Charging

Numerous anomalies have occurred from both surface and deep dielectric charging. Some of these have proved fatal (e.g. ANIK E1), while the more numerous, non-fatal anomalies enable the variations with Space Weather to be seen. The environmental parameters influencing charging have been reviewed in Ref. 28 from which the following figures are taken.
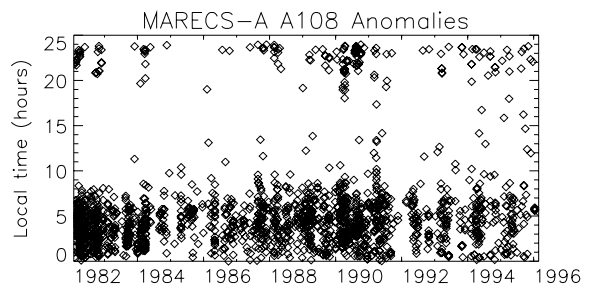

Figure 20. MARECS-A Anomalies vs year and local time

MARECS-A is a classic case of surface charging, as illustrated in figure 20 where anomalies can be seen to cluster during midnight to 0600 local time due to the eastwards drift of the enhanced electrons in the magnetotail during geomagnetic substorms. Enhanced rates around solar maximum are also seen.
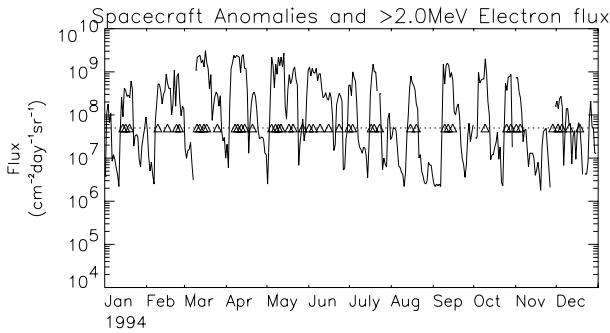
Figure 21. DRA-δ anomalies (Δ) & energetic electron fluxes.

DRA-δ anomalies are a classic example of deep dielectric charging and the rates correlate with energetic electron enhancements in the outer radiation belt. Figure 21 illustrates the huge variability in the outer zone and the presence of a 27- day recurrence period from fast solar wind streams. For this phenomenon there is evidence for enhanced rates towards solar minimum.

4. DISCUSSION

Cosmic radiation is responsible for single event effects in electronics and background noise in sensor systems. Production of atmospheric secondaries gives effects in aircraft systems and even in sea level electronics. The intensity is modulated in antiphase with the solar cycle and can undergo short term reductions due to solar wind variations.

Solar particle events are less energetic but more intense and can lead to greatly increased rates of SEE and noise as well as to significant dose and damage. The more energetic events can penetrate the atmosphere and provide significant enhancements in the radiation at supersonic aircraft altitudes. Prediction of their intensity, energy and composition is a challenge and this is further complicated by the influence of geomagnetic disturbances on their penetration of the magnetosphere.

The inner radiation belt comprises energetic protons and electrons and leads to dose, damage, noise and SEE. For most Low Earth Orbit situations the South Atlantic Anomaly region dominates and this is influenced by long term geomagnetic field evolution and by variations in the upper atmosphere density driven by solar radiation on both solar cycle and short term timescales.

The outer radiation belt comprises energetic electrons, which are highly dynamic and are driven by geomagnetic disturbances related to fast solar wind streams and coronal mass ejections. The prediction of cumulative dose and damage effects is thus complicated, while the large increases result in deep dielectric charging which is responsible for numerous anomalies and some losses. In addition geomagnetic disturbances produce less energetic plasma populations in the magnetotail and these have led to numerous surface charging anomalies.

The slot region can fill with energetic protons and electrons following certain geomagnetic disturbances and this leads to enhanced effects in certain orbits.

Space Weather variability makes predictions of effects difficult while future systems are likely to be more vulnerable due to use of higher performance digital electronics of increasing sensitivity. In addition there will be a decreasing supply of radhard components which were traditionally made available through military programmes. There is clearly a strong need for an active programme in Space Weather modelling, monitoring and prediction in order to ensure long-life, cost effective systems in Space and the upper atmosphere.

6. REFERENCES

1. J I Vette, "The NASA/National Space Science Data Center Trapped Radiation Environment Model Program (TREMP) (1964-1991)," NSSDC/WDC-A-R&S 91-29, NASA/GSFC, Nov 1991.
2. J I Vette, "The AE-8 Trapped Electron Model Environment," NSSDC/WDC-A-R&S 91-24, NASA/GSFC, Nov 1991.
3. L J Goldhammer, "Recent Solar Flare Activity And Its Effects On In-Orbit Solar Arrays," IEEE 21st PVSC, Vol II, 1241-1248, 1990.
4. A Jalinat, G Picart, E Rapp, P Samson, "In-Orbit Behaviour Of SPOT 1,2 and 3 Solar Arrays," ESA SP-416, 627-631, Sept 1998.
5. M A Shea, D F Smart , J H Allen, D C Wilkinson, "Spacecraft Problems in association with episodes of intense solar activity and related terrestrial phenomena during March 1991," IEEE Trans. Nuc. Sci., NS-39, 6, 1754-1760, Dec 1992.
6. B G Rax, C I Lee, A H Jonston, C E Barnes, "Total dose and proton damage in optocouplers," IEEE Trans. Nuc. Sci., NS-43, 6, 3167-3173, Dec 1996.
7. D C Wilkinson, S C Daughtridge, J L Stone, H H Sauer, P Darling, "TDRS-1 Single Event Upsets And The Effect Of The Space Environment," IEEE Trans. Nuc. Sci., 38, 6, 1708-1712, Dec 1991.
8. L Adams, E Daly, R Harboe-Sorenson, R Nickson, J Haines, W Shafer, M Conrad, H Greich, J Merkel, T Scwall, R Henneck, "A Verified Proton Induced Latch-Up In Space," IEEE Trans. Nuc. Sci., 39, 6, 1804-1808, Dec. 1992.
9. M Martigno, R Harboe-Sorenson, "IBM ThinkPad Radiation Testing And Recovery During EUROMIR Missions," IEEE Trans. Nuc. Sci. , 42, 6, 2004-2009, Dec 1995.
10. A L Klausman, "Effects Of Space Flight On Small Portable Computers," MSc Thesis, University of Houston at Clear Lake, Dec 1995.
11. A Sims, C Dyer, C Peerless, K Johansson, H Pettersson, J Farren,"The single event upset environment for avionics at high latitude", IEEE Trans. on Nuc. Sci., 41, 6, pp 2361-2367, Dec 1994.
12. C S Dyer, A J Sims, J Farren, J Stephen, "Measurements of the SEU environment in the upper atmosphere," IEEE Trans. on Nuc. Sci., NS-36, No 6, pp 2275-2280, Dec. 1989.
13. C S Dyer, A J Sims, J Farren, J Stephen, C Underwood,"Comparative measurements of the single event upset and total dose environments using the CREAM instruments", IEEE Trans.on Nuc. Sci., NS-39, No 3, pps 413-417, June 1992.
14 C Tsao, R Silberberg, J Adams Jr, J Letaw,"Cosmic ray effects on microelectronics:Part III:Propagation of cosmic rays in the atmosphere", NRL Memorandum Report 5402, Aug 1984.
15. C S Dyer & P R Truscott, "Cosmic radiation effects on avionics," ERA Technology Conference Volume for 1997 Avionics Conference, Heathrow UK, pp 6.3.1-6.3.10, November 1997.
16. J Olsen, P E Becher, P B Fynbo, P Raaby, J Schultz, "Neutron Induced Single Event Upsets In Static RAMs

Observed at 10 km Flight Altitude," IEEE Trans. Nuc. Sci., 40, 2, 74-77, April 1993.

17. A Taber, E Normand, "Single Event Upset In Avionics," IEEE Trans. Nuc. Sci. , 40, 2, 120-125, April 1993.

18. J H Adams,Jr., "Cosmic Ray Effects On Microelectronics, Part 1, The Near-Earth Particle Environment," NRL Memorandum Report 4506, Aug 1981.

19. C S Dyer, P R Truscott, C L Peerless, C J Watson, H E Evans, P Knight, M Cosby, C Underwood, T Cousins, R Noulty, "Updated measurements from CREAM & CREDO & implications for environment and shielding models," IEEE Trans. Nuc. Sci., NS-45, 3, 1584-1588, June 1998.

20. C Underwood, E Daly, R Harboe-Sorensen," Observation and analysis of single-event upset phenomena on-board the UOSAT-2 Satellite", Proceedings of the ESA Space Environment Workshop, ESTEC, Oct 1990.

21. C I Underwood, M K Oldfield, C S Dyer, A J Sims, " Long-term trend in the LEO radiation environment as measured by radiation monitors on-board three UoSAT-class micro-satellites," ESA SP-392, 37-44, Sept 1996.

22. A J Tylka, W F Dietrich, P R Boberg, E C Smith, J H Adams, Jr., "Single event upsets caused by solar energetic heavy ions," IEEE Trans. Nuc. Sci., NS-43, 6, pp 2758-2766, Dec 1996.

24. J B Blake, M S Gussenhoven, E G Mullen, and R W Fillius," Identification of an unexpected radiation hazard," IEEE Trans on Nuc Sci, NS-39, No 6, pp 1761-1764, Dec 1992.

25. M Gussenhoven, E Mullen, M Sperry, K Kerns, J Blake," The effect of the March 1991 storm on accumulated dose for selected satellite orbits: CRRES dose models", IEEE Trans. Nuc. Sci., 39, 6, pp 1765-1772, Dec 1992.

26. C S Dyer, P R Truscott, H E Evans, N Hammond, C Comber, S Battersby,"Calculations and observations of induced radioactivity in spaceborne materials", IEEE Trans. Nuc. Sci., 41, 3, pp 438-444, June 1994.

27. C S Dyer, P R Truscott, H E Evans, C L Peerless, "Simulation of spacecraft secondary particle emissions & their energy deposition in CCD X-ray detectors," IEEE Trans. Nuc. Sci., NS-43, 6, 2709-2714, Dec 1996.

28. G L Wrenn, R J K Smith , "Probability factors governing ESD effects in geosynchronous orbit," IEEE Trans. Nuc. Sci., NS-43, 6, pp 2783-2789, Dec 1996.

23. E Mullen, M Gussenhoven, K Ray, M Violet,"A double-peaked inner radiation belt: cause and effect as seen on CRRES", IEEE Trans. on Nuc. Sci., 38, 6, pp 1713-1717, Dec 1991.